

---

# InnerQ: Hardware-aware Tuning-free Quantization of KV Cache for Large Language Models

---

Mohammadreza Tayaranian\* Amir Ardakani Warren J. Gross  
 Department of Electrical and Computer Engineering  
 McGill University  
 Montreal, QC, Canada

## Abstract

Reducing the hardware footprint of large language models (LLMs) during decoding is critical for efficient long-sequence generation. A key bottleneck is the key-value (KV) cache, whose size scales with sequence length and easily dominates the memory footprint of the model. Previous work proposed quantization methods that are focused on compressing the KV cache while maintaining its information. We introduce InnerQ, a hardware-aware KV-cache quantization scheme that lowers decode latency without sacrificing accuracy. InnerQ applies group-wise quantization while grouping the cache matrices over their inner dimension. Unlike previous work that group over the outer dimension, InnerQ aligns dequantization with the vector-matrix multiplication and enables scale factor reuse across GPU compute units. This reduces memory accesses and accelerates dequantization, yielding up to 22% speedup over previous work and up to 88% over half-precision vector-matrix multiplication. To preserve fidelity under aggressive compression, InnerQ incorporates (i) hybrid quantization, selecting symmetric or asymmetric quantization per group based on local statistics; (ii) high-precision windows for both the most recent tokens and the attention sink tokens to mitigate outlier leakage; and (iii) per-channel normalization of the key cache, computed once during prefill and folded into the query to avoid runtime overhead. Our evaluation experiments on Llama models shows that InnerQ maintains a few-shot GSM8K performance comparable to non-quantized KV caches and surpasses prior KV cache quantization methods.

## 1 Introduction

Reducing the hardware requirements of text generation with LLMs incentivizes researchers to improve the efficiency of running these models. LLMs spend a considerable portion of their time in the decode phase, where they generate tokens one by one. As a result, the decode phase plays a major role in their overall efficiency [10]. KV caching is a widely-used method for increasing the throughput and reducing the memory overhead of LLMs in the decode phase [9]. It uses the cached key and value matrices of previous tokens and only computes the key and value of the most recent token. However, the size of the KV cache grows with each new token and quickly becomes the largest component of the model [7]. This emphasizes the importance of reducing the size of the KV cache to enable the use of LLMs for long-sequence generation.

Previous work proposed to use quantization to compress the KV cache [8, 6, 5, 13]. To better understand the dynamics of KV cache quantization in the decode phase, consider the vector-matrix multiplication  $C = AB$  between the non-quantized vector  $A \in \mathbb{R}^{1 \times K}$  and the quantized matrix  $B \in \mathbb{R}^{K \times N}$  where  $B$  can be either the key or the value and  $A$  can be either the query or the attention weights. Previous work applies group-wise quantization to  $B$  by breaking it into smaller groups and

---

\*Correspondence to mohammadreza.tayaranian@mail.mcgill.ca

scaling each group separately [8, 13]. One of the important factors in maintaining the precision in group-wise quantization is to avoid outlier values. To this end, quantization groups in previous work span over the outer dimension, i.e.  $N$  in the above example, to avoid including outliers in quantization groups [8, 13]. However, grouping the KV cache over the outer dimension is incompatible with the flow of the vector-matrix multiplication where each row of the cache matrix is dequantized and multiplied by the floating-point vector. In the case of outer dimension grouping, cells in each row are part of different quantization groups and are dequantized separately (Figure 2b). On the other hand, grouping over the inner dimension requires fewer memory accesses and enables the compute units to share the scale factors (Figure 2a). This leads to fewer memory accesses in the case of inner dimension grouping and decreases its overall latency compared to outer dimension grouping.

We propose InnerQ as a KV cache quantization method that is more hardware-aware and is focused on reducing the latency of the attention mechanism. InnerQ is comprised of different techniques where each technique is chosen to either reduce the latency or at least leave it unaffected:

- **Inner Dimension Grouping:** At its core, InnerQ applies group-wise quantization to the KV cache while applying the grouping over the *inner* dimension of the cache matrices. As noted above, grouping the cache matrices over their inner dimension leads to a lower number of memory accesses and speeds up the dequantization process. Our experimental results, reported in Figure 3b, compares the latency of vector-matrix multiplication with inner dimension grouping versus outer dimension grouping and demonstrates that inner dimension grouping is up to 22% faster.
- **Hybrid Quantization:** We propose a hybrid quantization mode and incorporate it into InnerQ. Hybrid quantization allows each quantization group to dynamically choose either symmetric or asymmetric quantization based on the values of each group. Given the varying distribution of the cache values, this allows the quantization to better adapt to the outliers. Despite requiring extra steps for finding the optimal quantization mode, hybrid quantization does not negatively affect the latency of the quantization process as the extra compute is performed in a memory-bound operation. Figure 4 demonstrates experimental results that verify our assumption regarding the effect of hybrid quantization on the latency.
- **High-precision Windows:** Inspired by previous work [8, 2], InnerQ keeps a small subset of cache tokens in a high-precision data type. Unlike KIVI [8] that fully devotes this window to the most recent tokens, we use some of the budget of the high-precision window towards the first few tokens of the sequence. The idea behind this design choice is to keep the attention sinks in a high-precision data type and avoid their leakage into the quantization groups [11].
- **Per-channel Normalization of Key Cache:** To reduce the magnitude of the outliers, InnerQ normalizes the key cache along the channel dimension. The normalization factor is computed during the prefill stage and is incorporated to the key and query weights to avoid adding an overhead to the attention mechanism.

We apply InnerQ to different variations of Llama [12, 4] and run few-shot evaluation on the GSM8k dataset [1]. Our experimental results, reported in Table 1, show that InnerQ results in an evaluation performance superior to previous work and comparable with the model with non-quantized KV cache. As reported in Figure 3, InnerQ’s use of inner dimension grouping reduces the latency of the vector-matrix multiplications of the KV cache by up to 88% and 22% compared to half-precision vector-matrix multiplication and vector-matrix multiplication where the quantized matrix is grouped over the outer dimension, respectively.

## 2 Related Work

KIVI [8] is one of the earliest works that proposes a tuning-free KV cache quantization method. It cites channel outliers as the main challenge in KV cache quantization and proposes an asymmetric quantization over the *outer* dimension of the key and value matrices to address this challenge. While we also propose a tuning-free quantization method with minimal overhead, we focus on quantizing the KV cache over the *inner* dimension for a higher speed up.

GEAR [6] uses low-rank decomposition alongside quantization to address the outlier challenge. Despite its low accuracy drop, its need to solve small optimization problems for the low-rank decomposition leads to runtime overheads. It proposes a CUDA implementation to further mitigate

this overhead. SQuat [13] proposes to minimize the quantization error by quantizing the key matrix such that its quantization error is orthogonal to the query. Built on top of KIVI, SQuat requires solving an optimization problem periodically to find the orthogonal matrix. Similar to GEAR, this extra optimization leads to improved accuracy, while negatively affecting the throughput of the quantized attention. Unlike GEAR and SQuat, our proposed method does not add extra steps to the quantization and is shown to have negligible overhead compared to KIVI.

KVQuant [5] proposes a non-uniform quantization where the quantization signposts are learned for each tensor. It uses a calibration dataset to compute the fisher matrix and find the signposts before inference begins. SKVQ [2] uses per-token group-wise quantization with dynamic clipping for both key and value. In other words, while key is quantized over the inner dimension, value is quantized over the outer dimension. Similar to our work, they propose to keep the most recent tokens in floating-point for higher precision. To overcome the outlier channels SKVQ proposes a custom ordering of channels. The optimal ordering of channels is found by gathering features of channels on a calibration dataset and clustering similar channels together for a smoother quantization. They also propose a variable group size which enables them to group similar channels together. However, whether their variable group size efficiently makes use of the resources in a general purpose GPU is not demonstrated by the authors. While calibration is an important step for both SKVQ and KVQuant, it leads to extra overhead and also makes their method reliant on external data. Unlike these methods, our proposed method dynamically adapts to data with hybrid quantization (Section 4.1.2) and does not require any extra calibration.

### 3 Background

#### 3.1 General Notation

Consider matrix  $A \in \mathbb{R}^{M \times K}$ . We use a slicing notation similar to PyTorch where we denote the  $i$ -th row and the  $j$ -th column of  $A$  as  $A_{i,:}$  and  $A_{:,j}$ , respectively. We denote the sub-matrix formed by concatenating rows  $i_1$  to  $i_2$  (inclusive) of  $A$  as  $A_{i_1:i_2,:}$ . Similarly, for the sub-matrix formed by concatenating columns  $j_1$  to  $j_2$  (inclusive) of  $A$  as  $A_{:,j_1:j_2}$ . The notation  $A_{i_1,:}$  describes the sub-matrix formed by concatenating rows  $i_1$  to the last row (inclusive). Similarly, the notation  $A_{:,i_1}$  describes the sub-matrix formed by concatenating from the first row to the  $i_1$ -th row (inclusive). For two matrices  $A \in \mathbb{R}^{N \times K}$  and  $B \in \mathbb{R}^{M \times K}$ , we denote their vertical concatenation (along the first dimension) as  $[A; B] \in \mathbb{R}^{(N+M) \times K}$ .

#### 3.2 KV Caching

The multi-head attention (MHA) is one of the building blocks of transformer-based large language models. It starts by transforming the hidden states  $h$  to  $Q \in \mathbb{R}^{N_Q, d}$  and to  $K$  and  $V \in \mathbb{R}^{N_K, d}$  as

$$Q = hW_Q \tag{1}$$

$$K = hW_K \quad V = hW_V. \tag{2}$$

It divides these matrices along the  $d$  dimension between  $n_h$  attention heads and computes the attention matrix,  $O \in \mathbb{R}^{N_Q, d}$ , as

$$S = QK^\top \tag{3}$$

$$P = \text{softmax}\left(\frac{S}{\sqrt{d_h}}\right) \tag{4}$$

$$O = PV \tag{5}$$

where  $d_h = \frac{d}{n_h}$  is the head dimension and  $n_h$  is the number of attention heads.

When a language model is used for language generation its operation is divided into two stages of *prefill* and *decode*. During the prefill stage the hidden states  $h \in \mathbb{R}^{N_Q, d}$  contain multiple tokens that help the model obtain the context of the current task. After prefill, the model enters the decode stage where it generates tokens one by one ( $N_Q = 1$ ). Despite that, key and value matrices contain all the context from the prefill stage and the decode stage up to that point ( $N_K > 1$ ).

Since the size of these matrices grow with every new token, KV caching proposes to cache and reuse key and value matrices to avoid their recomputation for each step. KV cache matrices are initialized

at the end of the prefill stage as

$$K_{\text{cache}} = K \quad V_{\text{cache}} = V \quad (6)$$

and are re-used for the subsequently generated tokens so that at each step of the decode phase the key and value is computed only for the last token. Using KV caching, Equation 2 is re-written as

$$K = [K_{\text{cache}}; hW_K] \quad V = [V_{\text{cache}}; hW_V]. \quad (7)$$

After each decode step, the cache is updated with the most recently computed key and value. This technique speeds up the generation process by avoiding the full linear transformation that creates the full  $K$  and  $V$  for each token.

### 3.3 KV Cache Quantization

Previous work proposed to quantize the KV cache to reduce its memory footprint. Given that both  $K$  and  $V$  are multiplied by full-precision matrices, KV cache quantization methods keep them in low-precision datatypes, but dequantize them before the matrix multiplications of Equations 3 and 5. Applying quantization to the KV cache, Equation 6 is reformulated as

$$\hat{K}_{\text{cache}} = \text{quant}(K) \quad \hat{V}_{\text{cache}} = \text{quant}(V) \quad (8)$$

and Equation 7 is replaced by

$$K = [\text{dequant}(\hat{K}_{\text{cache}}); hW_K] \quad V = [\text{dequant}(\hat{V}_{\text{cache}}); hW_V]. \quad (9)$$

where  $\hat{K}_{\text{cache}}$  and  $\hat{V}_{\text{cache}}$  are quantized cache matrices.

## 4 Methodology

### 4.1 Quantization Scheme

We propose to use  $b$ -bit group-wise quantization for  $K, V \in \mathbb{R}^{N_K \times d}$  with a group size  $G$ . Each matrix is divided into smaller quantization groups where values of each group share the same scale factor.

We begin by describing the symmetric and asymmetric quantization modes and then describe our proposed hybrid quantization mode. Without loss of generality we assume that the matrices are grouped over the last dimension ( $d \equiv 0 \pmod{G}$ ).  $K$  and  $V$  are interchangeable in the equations and definitions but we use  $K$  here for ease of reading.

#### 4.1.1 Asymmetric and Symmetric Quantization

Given  $S \in \mathbb{R}^{N_K \times \frac{d}{G}}$  as the scale factor matrix, and  $Z \in \mathbb{R}^{N_K \times \frac{d}{G}}$  as the zero-point matrix, the quantized value of the  $i$ -th row and the  $j$ -th column of  $K$  is calculated as

$$\hat{K}_{i,j} = \text{quant}_{\text{asym}}(K_{i,j}) = \text{clip}(\lfloor \frac{K_{i,j} - Z_{i,g}}{S_{i,g}} \rfloor, 0, 2^b - 1) \quad (10)$$

where  $\lfloor \cdot \rfloor$  is the round to nearest function and  $g = \lfloor (j-1)/G \rfloor$  is the group index of  $K_{i,j}$ . The zero point of the  $g$ -th group of the  $i$ -th row is computed as  $Z_{i,g} = \min(\mathcal{G}_{i,g})$  and its scale factor as

$$S_{i,g} = \frac{\max(\mathcal{G}_{i,g}) - Z_{i,g}}{2^b - 1} \quad (11)$$

where  $\mathcal{G}_{i,g} = \{K_{i,j} | \lfloor (j-1)/G \rfloor = g\}$  is the set of values in the group. As the values are shifted by their minimum, for all  $i$  and  $j$  we have  $0 \leq \hat{K}_{i,j}$  and thus  $\hat{K}$  is represented with an unsigned data-type.

Similarly,  $\hat{K}_{i,j}$  is dequantized as

$$\text{dequant}_{\text{asym}}(\hat{K}_{i,j}) = S_{i,g} \hat{K}_{i,j} + Z_{i,g}. \quad (12)$$

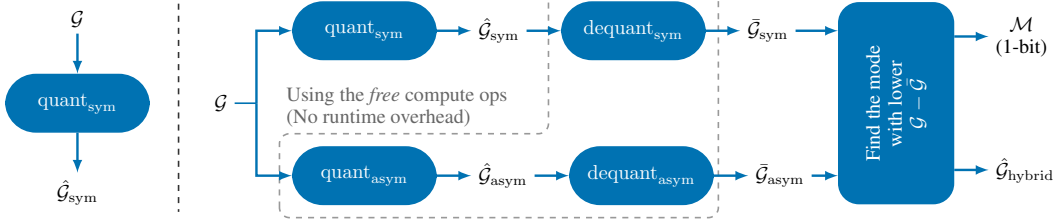


Figure 1: Depiction of the quantization process in symmetric quantization (left) and hybrid quantization (right) modes.  $\hat{\mathcal{G}}_{\text{hybrid}}$  is the output of the quantization mode with the lower error and  $\mathcal{M}$  is the quantized matrix from the mode with the lower error. The operations contained by the dashed gray line impose no additional overhead as they are working on the already loaded data in a memory bound operation.

Symmetric quantization is almost identical to asymmetric quantization except that it assumes a zero point of 0 for all groups. Consequently, the quantization and the dequantization process can be described using Equations 10 and 12 with  $Z_{i,g} = 0$ . The scale factor of each group is calculated by finding the absolute largest value as

$$S_{i,g} = \frac{\max(|\mathcal{G}_{i,g}|)}{2^b - 1} \quad (13)$$

where  $|\cdot|$  is the absolute value operator. Here, unlike asymmetric quantization, quantized values can be either negative or positive and are represented using signed data-types.

#### 4.1.2 Hybrid Quantization

Both asymmetric and symmetric quantization modes make assumptions about the data that they quantize. The degree to which these assumptions hold affects the accuracy of the quantized data. To better illustrate this point consider a quantization group  $\mathcal{G}$  for which  $\min(\mathcal{G}) > 0$ . Symmetric quantization uses a zero sign bit for all the values in this group. However, as asymmetric quantization assumes all the values are positive, it uses the available bits more efficiently to represent the values instead of their signs. As shown in Figure 2 in [8] the distribution of the values varies across different models and different layers. This observation points out that the optimal choice between symmetric and asymmetric quantization depends on the setup. Our experimental results in Table 6.1 confirms the sensitivity of the evaluation performance of the model to changing the quantization mode.

To adapt to this sensitivity, we propose a hybrid quantization mode that chooses the quantization mode between symmetric and asymmetric for each group. Recall from Section 4.1.1 that we denote the values in the  $g$ -th group of the  $i$ -th row as  $\mathcal{G}_{i,g}$ . We define a binary mask  $\mathcal{M}^{\text{sym}} \in \{0, 1\}^{N_K \times \frac{d}{G}}$  where  $\mathcal{M}_{i,g}^{\text{sym}}$  indicates whether the group is quantized using symmetric or asymmetric quantization.

based on the assumption that the quantization is a memory-bound process, we directly find  $\mathcal{M}_{i,g}^{\text{sym}}$  for each group. Since the overall latency of a memory bound process is dictated by the memory operations, a certain number of *free* operations can be executed on the already loaded data. These operations are free in the sense that their execution does not affect the latency of the process and are executed while the kernel waits for the next batch of data. As shown in Figure 1, for each quantization group, hybrid quantization uses the *free* compute budget to directly measure the quantization error for both asymmetric and symmetric quantization modes. It returns the quantized matrix with the lower error along with  $\mathcal{M}_{i,g}^{\text{sym}}$  to determine the chosen mode. We verify the validity of our assumption regarding the free compute budget by conducting experiments and measuring the latency of the hybrid and symmetric quantization functions in Section 5.3.

Given the irregular pattern of  $\mathcal{M}$ , we need a unified representation for quantized data to store the quantized values for both quantization modes. As discussed in Section 4.1.1, unlike symmetric quantization, asymmetric quantization attributes a zero point to each group. Another difference in their representation is the use of signed data types by symmetric quantization as opposed to an unsigned data type by asymmetric quantization. We propose a unified representation by separating the sign bit of the symmetrically quantized groups and packing them into one  $G$ -bit integer for each

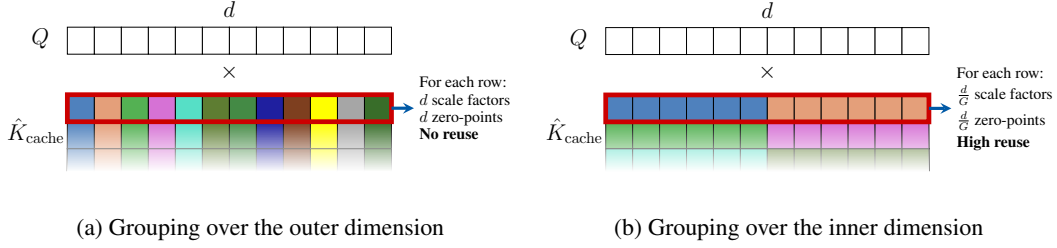


Figure 2: Visualization of the vector-vector multiplication between the floating-point vector  $Q$  and one row of the quantized matrix  $\hat{K}_{\text{cache}}$  in an illustrative example. Cells with the same color are in the same quantization group and share a scale factor and zero point. A similar visualization is true for the vector  $P$  and the quantized matrix  $\hat{V}_{\text{cache}}$ .

group. Throughout this work we assume a group size of 32 and an FP32 zero point which allows us to store the signs of symmetric groups and zero points of asymmetric groups in a unified manner in data types with the same bit-width. Using this representation, the memory footprint of hybrid quantization remains the same as either symmetric or asymmetric quantization with the exception of the overhead to store  $\mathcal{M}$ .

## 4.2 High-precision Window

As shown in previous work, keeping a small window of KV cache tokens in high precision greatly helps maintain model accuracy [8, 2]. We keep the last  $w_{\text{recent}}$  tokens in high precision and denote them as  $K_{\text{recent}}$  and  $V_{\text{recent}}$ . Similarly, the first  $w_{\text{sink}}$  tokens are also kept in another high precision window referred to as  $K_{\text{sink}}$  and  $V_{\text{sink}}$ . Given that finding the exact token in which the attention sinks appear requires extra computation overhead [11, 2], we set a fixed  $w_{\text{sink}}$  for all setups.

Incorporating the high-precision windows in Equation 8, we have

$$\begin{aligned}
 K_{\text{sink}} &= K_{:w_{\text{sink}},:} & V_{\text{sink}} &= V_{:w_{\text{sink}},:} \\
 K_{\text{recent}} &= K_{-w_{\text{recent}},:} & V_{\text{recent}} &= V_{-w_{\text{recent}},:} \\
 \hat{K}_{\text{cache}} &= \text{quant}(K_{w_{\text{sink}}:-w_{\text{recent}},:}) & \hat{V}_{\text{cache}} &= \text{quant}(V_{w_{\text{sink}}:-w_{\text{recent}},:}).
 \end{aligned} \tag{14}$$

During the decode phase,  $K_{\text{sink}}$  and  $V_{\text{sink}}$  are not modified but the computed  $K$  and  $V$  of each new token is appended to  $K_{\text{recent}}$  and  $V_{\text{recent}}$ . As new tokens are added to  $K_{\text{recent}}$  and  $V_{\text{recent}}$ , we quantize their oldest tokens and append them to  $\hat{K}_{\text{cache}}$  and  $\hat{V}_{\text{cache}}$ .

## 4.3 Per-channel Normalization of $K$

The presence of an outlier in a quantization group leads to the loss of precision for other values. On the other hand, previous work showed that outliers emerge across the channel dimension of  $K$  [8]. We dampen the outliers by applying per-channel normalization to  $K$ . Note that per-channel normalization is possible only when quantization groups in  $K$  span across different channels, i.e. per-token group-wise quantization.

The normalization factor for channel  $1 \leq i \leq d$  is computed as  $\text{norm}_i^K = \sqrt{\max(|K_{:,i}|)}$  where  $|\cdot|$  the absolute value.  $\text{norm}_i^K$  is computed at the end of the prefill stage and is used to normalize  $K$  just before Equation 8. We incorporate  $\text{norm}_i^K$  into  $W_Q$  and  $W_K$  to keep the attention operations mathematically equivalent and minimize the normalization overhead.

## 4.4 InnerQ: Quantizing Key and Value Over the Inner Dimension

As shown in Equation 9,  $K_{\text{cache}}$  and  $V_{\text{cache}}$  are dequantized at every step before being multiplied by other matrices. In a naive implementation separate kernel calls are invoked for this process: one for Equation 9 and the other for the matrix multiplication that follows it, i.e. Equations 3 and 5. Previous work proposed to reduce the overhead of separate kernel calls by using a single fused kernel that dequantizes each group on the fly and then performs matrix multiplication on it [8].

Quantization Mode	Llama 3.2-1B	Llama 2-7B	Llama 3.1-8B	Llama 2-13B
Baseline	5.84% (32.5 MB)	13.12% (637.5 MB)	51.02% (128.7 MB)	24.34% (1003.5 MB)
KIVI [8]	4.09% (10.4 MB)	12.74% (191.9 MB)	45.56% (41.3 MB)	24.11% (301.4 MB)
KIVI+sink	5.38% (10.4 MB)	13.12% (191.9 MB)	49.20% (41.3 MB)	24.41% (301.4 MB)
InnerQ (ours)	5.69% (10.4 MB)	13.64% (193.0 MB)	49.58% (41.5 MB)	24.87% (303.2 MB)

Table 1: Exact-match metric of different Llama models on the evaluation set of GSM8k under different KV cache quantization regimes. For each setup, the average size of the KV cache is shown in parentheses.

KV cache quantization is applied in the decode stage where  $N_Q = 1$  and Equations 3 and 5 are both vector-matrix multiplications. For Equation 3, the above mentioned fused kernel iterates over rows of  $K$  and performs the vector-vector multiplication to compute the output. As depicted in Figure 2a, when grouped over its inner dimension, i.e.  $N$ , values of the same group in each row of  $K$  share the same scale factor and each scale factor is reused for multiple operations, leading to a higher throughput<sup>2</sup>. On the other hand, Figure 2b shows that if  $K$  is grouped over the outer dimension, multiple scale factors are loaded per row that are not shared between the cells in each row. A similar argument is valid for Equation 5 where  $P$  is a floating-point vector and  $V$  a quantized matrix. Figure 3b confirms this hypothesis and shows that grouping over the inner dimension increases the throughput of the quantized matrix-multiplication.

Despite its higher latency, previous work grouped the KV cache over the outer dimension to avoid the accuracy drops caused by outlier channels. Although we make a similar observation regarding the pattern of outliers, we quantize the KV cache by applying the hybrid quantization introduced in Section 4.1.2 on  $K$  and  $V$  while grouping them over their *inner* dimension. This means that we apply per-token group-wise quantization to  $K$  and per-channel group-wise quantization to  $V$ . Following Section 4.2, we keep two full-precision windows for recent and sink tokens, respectively. We also apply per-channel normalization as outlined in Section 4.3 to  $K$  to flatten the outliers. Appendix A provides a more in-depth view into the inner workings of the attention computation with InnerQ.

## 5 Experiments

### 5.1 Setup

We apply InnerQ to different sizes and versions of Llama [12, 4] and observe its effect on the evaluation performance of the model with quantized KV cache. We implement a quantized KV cache based on the HuggingFace Transformers library and use the LM-eval [3] framework to build our evaluation script. For the baseline, we include a setup where KV cache is not quantized. We also compare our results with KIVI [8] as the most-prominent tuning-free KV cache quantization method. For a better comparison, we provide an additional setup denoted as KIVI+sink by devoting some of the high-precision window tokens of KIVI to cover the sink tokens. Following previous work, we set the group size to 32 and the total length of the high-precision window to 128. In the KIVI+sink and InnerQ setups we have  $w_{\text{sink}} = 32$  and  $w_{\text{recent}} = 96$  and for the KIVI setup we have  $w_{\text{sink}} = 0$  and  $w_{\text{recent}} = 128$ . The bit-width of the quantized KV cache in all quantized setups is set to 2. We turn off the per-channel normalization in InnerQ for the experiments using Llama 2-13B based on our hyper-parameter search. We report the metric `exact_match`, `flexible-extract` for all the setups and models.

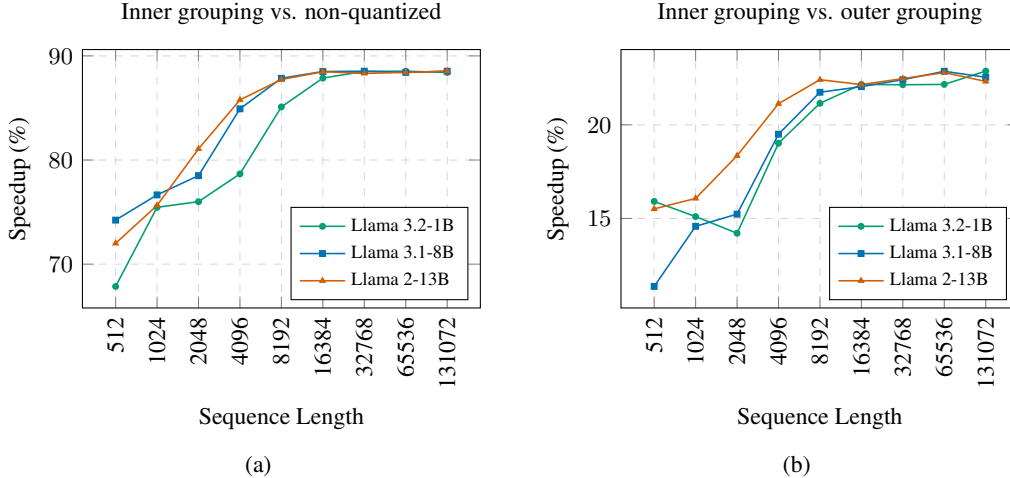


Figure 3: (a) Speedup of vector-matrix multiplication when the matrix is quantized to 2 bits and grouped over the inner dimension versus when the matrix is in half-precision and multiplied using `torch.matmul`. (b) Speedup of the vector-matrix multiplication with the 2-bit quantized matrix grouped over the inner dimension versus the outer dimension.

## 5.2 Evaluation Performance and Cache Size

We compare the performance of InnerQ with other setups by applying them to pre-trained models and running few-shot evaluation on the evaluation set of the GSM8k dataset [1]. As reported in Table 1, InnerQ maintains the metric performance of the baseline while significantly reducing the size of the KV cache. InnerQ also shows a superior evaluation performance compared to both KIVI variants while having a slightly higher cache size due to mask used by hybrid quantization. We study the trade-off of the hybrid quantization mask in terms of memory usage and metric performance in Section 6.1.

## 5.3 Latency

As briefly mentioned in Section 4.4, grouping the quantized KV cache matrices over their inner dimension theoretically leads to lower latency. We test this hypothesis by implementing a Triton fused kernel for quantized vector-matrix multiplications and use it to compare the throughput of InnerQ against outer dimension quantization, e.g. KIVI [8]. Our kernels operate on quantized matrices and non-quantized vectors to simulate Equations 3 and 5 in the decode phase with quantized KV cache. We measure the latency of the quantized matrix-multiplication with a batch size of 1 on a machine with an NVIDIA RTX 4090 GPU. We begin by running the kernel 100 times to warm up the GPU. Each measured latency is the median of 1000 measurements. Figure 3b reports the speedup resulted by using inner dimension grouping compared with outer dimension grouping. It confirms our hypothesis that grouping over the inner dimension, used by InnerQ, is faster than grouping over the outer dimension across all models and sequence lengths. In all models, as the number of tokens increases, the speedup grows and reaches levels around 22%. We also compare the latency of the vector-matrix multiplication with inner dimension grouping against the half-precision vector-matrix multiplication in `torch.matmul`. Figure 3a shows the significant speedup of using our quantized vector-matrix multiplication compared to half-precision multiplication with speedup levels reaching up to 88%. We report the full latency measurements in Appendix B.

We also compare the latency of the quantization function of our proposed hybrid quantization against symmetric quantization. As discussed in Section 4.1.2 and depicted in Figure 1, the additional computation done by hybrid quantization does not affect the overall latency compared to uniform quantization. The intuition behind this claim is the assumption that quantization is a memory-bound operation. This means that the latency of a quantization kernel is determined by the latency of the memory operations. As a result, the extra compute of hybrid quantization, as long as it is performed

<sup>2</sup>A similar argument is valid for zero points in the case of asymmetric quantization.

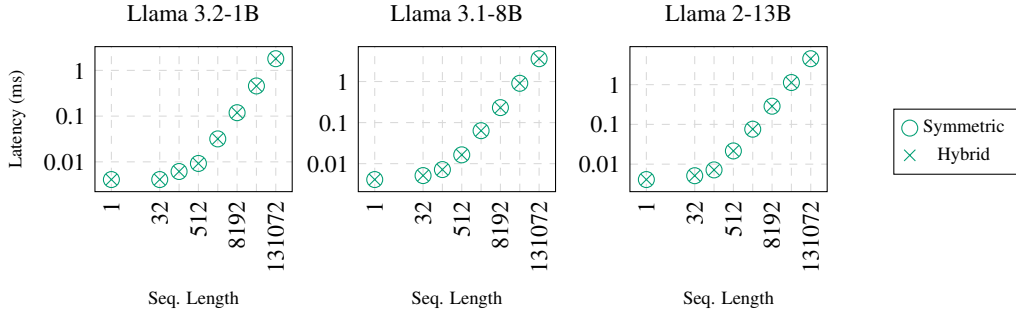


Figure 4: Latency of the quantization operation when using hybrid quantization versus symmetric quantization.

Quantization Mode	Llama 3.2-1B	Llama 2-7B	Llama 3.1-8B	Llama 2-13B
Asymmetric	4.02%	12.89%	46.40%	22.75%
Symmetric	5.16%	14.10%	48.90%	24.72%
Hybrid	5.69%	13.64%	49.58%	24.87%
Hybrid <sub>Prefill</sub>	5.69%	13.19%	49.96%	24.56%

Table 2: Effect of changing quantization mode of InnerQ on the evaluation performance of different Llama models on GSM8k.

on already loaded data, does not slow down the overall process. To verify this assumption, we implement a Triton kernel for both symmetric quantization and hybrid quantization and compare their latency in a setup similar to above. As shown in Figure 4 the latency of hybrid quantization and symmetric quantization is negligible across multiple models and sequence lengths, confirming that hybrid quantization and symmetric quantization have a similar latency.

## 6 Ablation Studies

### 6.1 Quantization Mode

Hybrid quantization gives InnerQ the flexibility of adapting to the quantized data by using extra compute during the quantization process to find the best quantization mode for each group. We have already shown in Section 5.3 that hybrid quantization does not incur extra latency overhead compared to other quantization modes. In this section we compare the memory footprint of hybrid quantization with uniform quantization methods. Recall from Section 4.1.2 that hybrid quantization uses a binary mask for each quantization group that needs to be stored as part of the KV cache. This mask is the main contributing factor to the difference in cache size between InnerQ and KIVI shown in Table 1.

We conduct experiments to better understand the trade-off between the extra memory usage of hybrid quantization and the additional model accuracy that it provides for the model. In these experiments we change the quantization mode of InnerQ while keeping other hyper-parameters the same. In addition to symmetric and asymmetric quantization, we introduce a new quantization mode and refer to it as Hybrid<sub>Prefill</sub>. Unlike hybrid quantization that adaptively chooses the quantization mode across the entire inference, Hybrid<sub>Prefill</sub> uses hybrid quantization only for the prefill stage and opts for symmetric quantization for the decode stage. As a result, unlike hybrid quantization where the mask grows with the sequence length, Hybrid<sub>Prefill</sub> limits the mask size to the number of tokens in the prefill stage. As shown in Table 2, unlike asymmetric quantization that leads to considerable performance drops, symmetric, hybrid, and Hybrid<sub>Prefill</sub> quantization modes all result in similar performance range with hybrid quantization leading to a higher average performance. Given that hybrid and Hybrid<sub>Prefill</sub> have additional memory requirements compared to symmetric quantization, the user can choose whether to accept the overhead for a higher evaluation performance or to save memory with the risk of losing the evaluation performance.

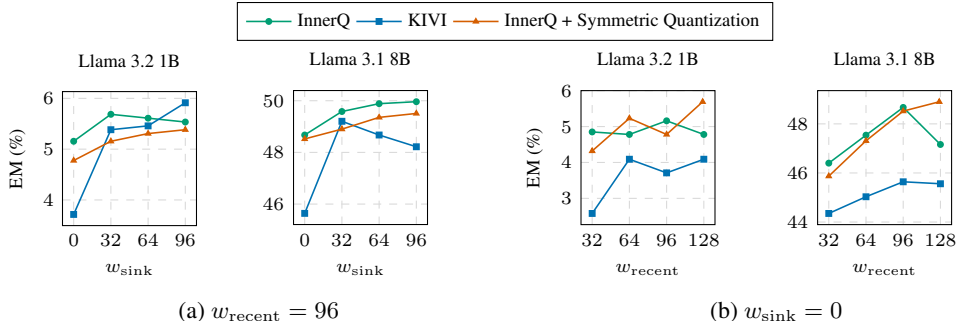


Figure 5: Effect of changing high-precision window length on the evaluation performance of Llama with quantized KV cache on GSM8k dataset.

## 6.2 High-precision Windows

We change the hyper-parameters  $w_{\text{sink}}$  and  $w_{\text{recent}}$  to study the effect of the high-precision windows on the evaluation performance of the models with quantized KV cache. As shown in Figure 5a, the absence of high-precision sink tokens, i.e.  $w_{\text{sink}} = 0$ , has a significant impact on the metric performance when using KIVI. On the other hand, InnerQ is less affected by the absence of sink high-precision window. As this resilience is observed for both the standard InnerQ and the setup with symmetric quantization, we attribute it to the fact that InnerQ quantizes the cache over the inner dimension. Figure 5b shows that increasing  $w_{\text{recent}}$  helps boost the performance of all quantization methods, with KIVI still lagging behind InnerQ.

## 7 Conclusion and Future Work

In this work we introduced InnerQ, a hardware-aware KV-cache quantization scheme. InnerQ yields up to 22% lower latency compared with common KV cache quantization methods and up to 88% versus the non-quantized baseline. This speedup is achieved by applying group-wise quantization where groups are spread over the inner dimension of the quantized matrices. This aligns the quantization layout with the execution flow of the vector-matrix multiplication and minimizes memory traffic and dequantization overhead. InnerQ augments this layout with per-group hybrid (symmetric/asymmetric) quantization, high-precision windows that protect both recent tokens and early attention sinks, and a per-channel key normalization. Across multiple Llama variants, these choices maintain few-shot GSM8K accuracy comparable to non-quantized KV caches and outperform prior KV cache quantization baselines while keeping the KV cache size comparable to previous KV cache quantization baselines. Overall, the main highlight of InnerQ is the importance of co-designing the quantization method with the hardware memory access patterns to maximize quantization speedups.

Future work will assess our method across a wider range of tasks and benchmarks. We will also systematically examine how our quantization scheme interacts with alternative KV cache eviction strategies. Another direction is to design adaptive and low-overhead policies for selecting tokens that are retained in the high-precision windows.

## References

- [1] K. Cobbe, V. Kosaraju, M. Bavarian, M. Chen, H. Jun, L. Kaiser, M. Plappert, J. Tworek, J. Hilton, R. Nakano, et al. Training verifiers to solve math word problems. *arXiv preprint arXiv:2110.14168*, 2021. doi: 10.48550/arXiv.2110.14168.
- [2] H. Duanmu, Z. Yuan, X. Li, J. Duan, X. ZHANG, and D. Lin. SKVQ: Sliding-window key and value cache quantization for large language models. In *First Conference on Language Modeling*, 2024. URL <https://openreview.net/forum?id=nI6JyFSnyV>.
- [3] L. Gao, J. Tow, B. Abbasi, S. Biderman, S. Black, A. DiPofi, C. Foster, L. Golding, J. Hsu, A. Le Noac’h, H. Li, K. McDonnell, N. Muennighoff, C. Ociepa, J. Phang, L. Reynolds,

H. Schoelkopf, A. Skowron, L. Sutawika, E. Tang, A. Thite, B. Wang, K. Wang, and A. Zou. A framework for few-shot language model evaluation, 07 2024. URL <https://zenodo.org/records/12608602>.

- [4] A. Grattafiori, A. Dubey, A. Jauhri, A. Pandey, A. Kadian, A. Al-Dahle, A. Letman, A. Mathur, A. Schelten, A. Vaughan, A. Yang, A. Fan, A. Goyal, A. Hartshorn, A. Yang, A. Mitra, A. Srivankumar, A. Korenev, A. Hinsvark, A. Rao, A. Zhang, A. Rodriguez, A. Gregerson, A. Spataru, B. Roziere, B. Biron, B. Tang, B. Chern, C. Caucheteux, C. Nayak, C. Bi, C. Marra, C. McConnell, C. Keller, C. Touret, C. Wu, C. Wong, C. C. Ferrer, C. Nikolaidis, D. Allonsius, D. Song, D. Pintz, D. Livshits, D. Wyatt, D. Esiobu, D. Choudhary, D. Mahajan, D. Garcia-Olano, D. Perino, D. Hupkes, E. Lakomkin, E. AlBadawy, E. Lobanova, E. Dinan, E. M. Smith, F. Radenovic, F. Guzmán, F. Zhang, G. Synnaeve, G. Lee, G. L. Anderson, G. Thattai, G. Nail, G. Mialon, G. Pang, G. Cucurell, H. Nguyen, H. Korevaar, H. Xu, H. Touvron, I. Zarov, I. A. Ibarra, I. Kloumann, I. Misra, I. Evtimov, J. Zhang, J. Copet, J. Lee, J. Geffert, J. Vranes, J. Park, J. Mahadeokar, J. Shah, J. van der Linde, J. Billock, J. Hong, J. Lee, J. Fu, J. Chi, J. Huang, J. Liu, J. Wang, J. Yu, J. Bitton, J. Spisak, J. Park, J. Rocca, J. Johnstun, J. Saxe, J. Jia, K. V. Alwala, K. Prasad, K. Upasani, K. Plawiak, K. Li, K. Heafield, K. Stone, K. El-Arini, K. Iyer, K. Malik, K. Chiu, K. Bhalla, K. Lakhotia, L. Rantala-Yeary, L. van der Maaten, L. Chen, L. Tan, L. Jenkins, L. Martin, L. Madaan, L. Malo, L. Blecher, L. Landzaat, L. de Oliveira, M. Muzzi, M. Pasupuleti, M. Singh, M. Paluri, M. Kardas, M. Tsimpoukelli, M. Oldham, M. Rita, M. Pavlova, M. Kambadur, M. Lewis, M. Si, M. K. Singh, M. Hassan, N. Goyal, N. Torabi, N. Bashlykov, N. Bogoychev, N. Chatterji, N. Zhang, O. Duchenne, O. Çelebi, P. Alrassy, P. Zhang, P. Li, P. Vasic, P. Weng, P. Bhargava, P. Dubal, P. Krishnan, P. S. Koura, P. Xu, Q. He, Q. Dong, R. Srinivasan, R. Ganapathy, R. Calderer, R. S. Cabral, R. Stojnic, R. Raileanu, R. Maheswari, R. Girdhar, R. Patel, R. Sauvestre, R. Polidoro, R. Sumbaly, R. Taylor, R. Silva, R. Hou, R. Wang, S. Hosseini, S. Chennabasappa, S. Singh, S. Bell, S. S. Kim, S. Edunov, S. Nie, S. Narang, S. Raparthy, S. Shen, S. Wan, S. Bhosale, S. Zhang, S. Vandenhende, S. Batra, S. Whitman, S. Sootla, S. Collot, S. Gururangan, S. Borodinsky, T. Herman, T. Fowler, T. Sheasha, T. Georgiou, T. Scialom, T. Speckbacher, T. Mihaylov, T. Xiao, U. Karn, V. Goswami, V. Gupta, V. Ramanathan, V. Kerkez, V. Gonguet, V. Do, V. Vogeti, V. Albiero, V. Petrovic, W. Chu, W. Xiong, W. Fu, W. Meers, X. Martinet, X. Wang, X. Wang, X. E. Tan, X. Xia, X. Xie, X. Jia, X. Wang, Y. Goldschlag, Y. Gaur, Y. Babaei, Y. Wen, Y. Song, Y. Zhang, Y. Li, Y. Mao, Z. D. Coudert, Z. Yan, Z. Chen, Z. Papakipos, A. Singh, A. Srivastava, A. Jain, A. Kelsey, A. Shajnfeld, A. Gangidi, A. Victoria, A. Goldstand, A. Menon, A. Sharma, A. Boesenberg, A. Baevski, A. Feinstein, A. Kallet, A. Sangani, A. Teo, A. Yunus, A. Lupu, A. Alvarado, A. Caples, A. Gu, A. Ho, A. Poulton, A. Ryan, A. Ramchandani, A. Dong, A. Franco, A. Goyal, A. Saraf, A. Chowdhury, A. Gabriel, A. Bharambe, A. Eisenman, A. Yazdan, B. James, B. Maurer, B. Leonhardi, B. Huang, B. Loyd, B. D. Paola, B. Paranjape, B. Liu, B. Wu, B. Ni, B. Hancock, B. Wasti, B. Spence, B. Stojkovic, B. Gamido, B. Montalvo, C. Parker, C. Burton, C. Mejia, C. Liu, C. Wang, C. Kim, C. Zhou, C. Hu, C.-H. Chu, C. Cai, C. Tindal, C. Feichtenhofer, C. Gao, D. Civin, D. Beaty, D. Kreymer, D. Li, D. Adkins, D. Xu, D. Testuggine, D. David, D. Parikh, D. Liskovich, D. Foss, D. Wang, D. Le, D. Holland, E. Dowling, E. Jamil, E. Montgomery, E. Presani, E. Hahn, E. Wood, E.-T. Le, E. Brinkman, E. Arcaute, E. Dunbar, E. Smothers, F. Sun, F. Kreuk, F. Tian, F. Kokkinos, F. Ozgenel, F. Caggioni, F. Kanayet, F. Seide, G. M. Florez, G. Schwarz, G. Badeer, G. Swee, G. Halpern, G. Herman, G. Sizov, Guangyi, Zhang, G. Lakshminarayanan, H. Inan, H. Shojanazeri, H. Zou, H. Wang, H. Zha, H. Habeeb, H. Rudolph, H. Suk, H. Aspegren, H. Goldman, H. Zhan, I. Damlaj, I. Molybog, I. Tufanov, I. Leontiadis, I.-E. Veliche, I. Gat, J. Weissman, J. Geboski, J. Kohli, J. Lam, J. Asher, J.-B. Gaya, J. Marcus, J. Tang, J. Chan, J. Zhen, J. Reizenstein, J. Teboul, J. Zhong, J. Jin, J. Yang, J. Cummings, J. Carvill, J. Shepard, J. McPhie, J. Torres, J. Ginsburg, J. Wang, K. Wu, K. H. U, K. Saxena, K. Khandelwal, K. Zand, K. Matosich, K. Veeraraghavan, K. Michelena, K. Li, K. Jagadeesh, K. Huang, K. Chawla, K. Huang, L. Chen, L. Garg, L. A. L. Silva, L. Bell, L. Zhang, L. Guo, L. Yu, L. Moshkovich, L. Wehrstedt, M. Khabsa, M. Avalani, M. Bhatt, M. Mankus, M. Hasson, M. Lennie, M. Reso, M. Groshev, M. Naumov, M. Lathi, M. Keneally, M. Liu, M. L. Seltzer, M. Valko, M. Restrepo, M. Patel, M. Vyatskov, M. Samvelyan, M. Clark, M. Macey, M. Wang, M. J. Hermoso, M. Metanat, M. Rastegari, M. Bansal, N. Santhanam, N. Parks, N. White, N. Bawa, N. Singhal, N. Egebo, N. Usunier, N. Mehta, N. P. Laptev, N. Dong, N. Cheng, O. Chernoguz, O. Hart, O. Salpekar, O. Kalinli, P. Kent, P. Parekh, P. Saab, P. Balaji, P. Rittner, P. Bontrager, P. Roux, P. Dollar,

- P. Zvyagina, P. Ratanchandani, P. Yuvraj, Q. Liang, R. Alao, R. Rodriguez, R. Ayub, R. Murthy, R. Nayani, R. Mitra, R. Parthasarathy, R. Li, R. Hogan, R. Battey, R. Wang, R. Howes, R. Rinott, S. Mehta, S. Siby, S. J. Bondu, S. Datta, S. Chugh, S. Hunt, S. Dhillon, S. Sidorov, S. Pan, S. Mahajan, S. Verma, S. Yamamoto, S. Ramaswamy, S. Lindsay, S. Feng, S. Lin, S. C. Zha, S. Patil, S. Shankar, S. Zhang, S. Zhang, S. Wang, S. Agarwal, S. Sajuyigbe, S. Chintala, S. Max, S. Chen, S. Kehoe, S. Satterfield, S. Govindaprasad, S. Gupta, S. Deng, S. Cho, S. Virk, S. Subramanian, S. Choudhury, S. Goldman, T. Remez, T. Glaser, T. Best, T. Koehler, T. Robinson, T. Li, T. Zhang, T. Matthews, T. Chou, T. Shaked, V. Vontimitta, V. Ajayi, V. Montanez, V. Mohan, V. S. Kumar, V. Mangla, V. Ionescu, V. Poenaru, V. T. Mihailescu, V. Ivanov, W. Li, W. Wang, W. Jiang, W. Bouaziz, W. Constable, X. Tang, X. Wu, X. Wang, X. Wu, X. Gao, Y. Kleinman, Y. Chen, Y. Hu, Y. Jia, Y. Qi, Y. Li, Y. Zhang, Y. Zhang, Y. Adi, Y. Nam, Yu, Wang, Y. Zhao, Y. Hao, Y. Qian, Y. Li, Y. He, Z. Rait, Z. DeVito, Z. Rosnbrick, Z. Wen, Z. Yang, Z. Zhao, and Z. Ma. The Llama 3 herd of models. *arXiv preprint arXiv:2407.21783*, 2024. doi: 10.48550/arXiv.2407.21783.
- [5] C. Hooper, S. Kim, H. Mohammadzadeh, M. W. Mahoney, Y. S. Shao, K. Keutzer, and A. Gholami. KVQuant: Towards 10 million context length LLM inference with KV cache quantization. In A. Globerson, L. Mackey, D. Belgrave, A. Fan, U. Paquet, J. Tomczak, and C. Zhang, editors, *Advances in Neural Information Processing Systems*, volume 37, pages 1270–1303. Curran Associates, Inc., 2024. doi: 10.52202/079017-0040.
- [6] H. Kang, Q. Zhang, S. Kundu, G. Jeong, Z. Liu, T. Krishna, and T. Zhao. GEAR: An efficient error reduction framework for KV cache compression in LLM inference. In M. Rezagholizadeh, P. Passban, S. Samiee, V. Partovi Nia, Y. Cheng, Y. Deng, Q. Liu, and B. Chen, editors, *Proceedings of The 4th NeurIPS Efficient Natural Language and Speech Processing Workshop*, volume 262 of *Proceedings of Machine Learning Research*, pages 305–321. PMLR, 14 Dec 2024. URL <https://proceedings.mlr.press/v262/kang24a.html>.
- [7] A. Liu, J. Liu, Z. Pan, Y. He, G. Haffari, and B. Zhuang. MiniCache: KV cache compression in depth dimension for large language models. In A. Globerson, L. Mackey, D. Belgrave, A. Fan, U. Paquet, J. Tomczak, and C. Zhang, editors, *Advances in Neural Information Processing Systems*, volume 37, pages 13997–140031. Curran Associates, Inc., 2024. doi: 10.52202/079017-4443. URL [https://proceedings.neurips.cc/paper\\_files/paper/2024/file/fd0705710bf01b88a60a3d479ea341d9-Paper-Conference.pdf](https://proceedings.neurips.cc/paper_files/paper/2024/file/fd0705710bf01b88a60a3d479ea341d9-Paper-Conference.pdf).
- [8] Z. Liu, J. Yuan, H. Jin, S. Zhong, Z. Xu, V. Braverman, B. Chen, and X. Hu. KIVI: A tuning-free asymmetric 2bit quantization for KV cache. *arXiv preprint arXiv:2402.02750*, 2024. doi: 10.48550/arXiv.2402.02750.
- [9] R. Pope, S. Douglas, A. Chowdhery, J. Devlin, J. Bradbury, J. Heek, K. Xiao, S. Agrawal, and J. Dean. Efficiently scaling transformer inference. In D. Song, M. Carbin, and T. Chen, editors, *Proceedings of Machine Learning and Systems*, volume 5, pages 606–624. Curran, 2023. URL [https://proceedings.mlsys.org/paper\\_files/paper/2023/file/c4be71ab8d24cdfb45e3d06dbfca2780-Paper-mlsys2023.pdf](https://proceedings.mlsys.org/paper_files/paper/2023/file/c4be71ab8d24cdfb45e3d06dbfca2780-Paper-mlsys2023.pdf).
- [10] R. Sanovar, S. Bharadwaj, R. S. Amant, V. Rühle, and S. Rajmohan. LeanAttention: Hardware-aware scalable attention mechanism for the decode-phase of transformers. In *Eighth Conference on Machine Learning and Systems*, 2025. URL <https://openreview.net/forum?id=KVZDNEoCOQ>.
- [11] Z. Su and K. Yuan. KVSink: Understanding and enhancing the preservation of attention sinks in KV cache quantization for LLMs. In *Second Conference on Language Modeling*, 2025. URL <https://openreview.net/forum?id=gIqb6zWZo0>.
- [12] H. Touvron, L. Martin, K. Stone, P. Albert, A. Almahairi, Y. Babaei, N. Bashlykov, S. Batra, P. Bhargava, S. Bhosale, D. Bikel, L. Blecher, C. C. Ferrer, M. Chen, G. Cucurull, D. Esiobu, J. Fernandes, J. Fu, W. Fu, B. Fuller, C. Gao, V. Goswami, N. Goyal, A. Hartshorn, S. Hosseini, R. Hou, H. Inan, M. Kardas, V. Kerkez, M. Khabsa, I. Kloumann, A. Korenev, P. S. Koura, M.-A. Lachaux, T. Lavril, J. Lee, D. Liskovich, Y. Lu, Y. Mao, X. Martinet, T. Mihaylov, P. Mishra, I. Molybog, Y. Nie, A. Poulton, J. Reizenstein, R. Rungta, K. Saladi, A. Schelten, R. Silva, E. M. Smith, R. Subramanian, X. E. Tan, B. Tang, R. Taylor, A. Williams, J. X. Kuan, P. Xu, Z. Yan, I. Zarov, Y. Zhang, A. Fan, M. Kambadur, S. Narang, A. Rodriguez, R. Stojnic,

S. Edunov, and T. Scialom. Llama 2: Open foundation and fine-tuned chat models. *arXiv preprint arXiv:2307.09288*, 2023. doi: 10.48550/arXiv.2307.09288.

- [13] H. Wang, L. Han, K. Xu, and A. Srivastava. Squat: Subspace-orthogonal KV cache quantization. *arXiv preprint arXiv:2503.24358*, 2025. doi: 10.48550/arXiv.2503.24358.

---

**Algorithm 1** Multi-head attention with quantized cache in the decode phase

---

**Require:** Input sequence  $X \in \mathbb{R}^{1 \times d}$

**Require:** Trainable weights  $W_Q, W_O, W_K, W_V \in \mathbb{R}^{d \times d}$

**Require:** Number of heads  $n_h$  and head dimension  $d_h = d/n_h$

**Require:** Quantization Group Size  $G$

```
1: procedure LLAMA3ATTENTION( $X$ )
2:
3:    $Q \leftarrow XW_Q$ 
4:    $K \leftarrow XW_K$ 
5:    $V \leftarrow XW_V$ 
6:    $Q, K \leftarrow \text{ApplyRoPE}(Q, K)$ 
7:    $K_{\text{recent}} \leftarrow \text{concat}(K_{\text{recent}}, K)$ 
8:    $V_{\text{recent}} \leftarrow \text{concat}(V_{\text{recent}}, V)$ 
9:
10:   $S \leftarrow [QK_{\text{recent}}^\top, \text{QuantizedMatmul}(Q, \hat{K}_{\text{cache}}^\top), QK_{\text{recent}}^\top]$ 
11:   $P \leftarrow \text{Softmax}((S/d_h) + \text{Mask})$ 
12:   $O \leftarrow PV_{\text{recent}} + \text{QuantizedMatmul}(P, \hat{V}_{\text{cache}}) + PV_{\text{recent}}$ 
13:   $O \leftarrow OW_O$ 
14:
15:   $\hat{K}_{\text{new}} \leftarrow \text{Quantize}(K_{\text{recent}}[:, G])$ 
16:   $K_{\text{recent}} \leftarrow K_{\text{recent}}[G : ]$ 
17:   $\hat{K}_{\text{cache}} \leftarrow \text{concat}(\hat{K}_{\text{cache}}, \hat{K}_{\text{new}})$ 
18:
19:  if nb_tokens( $V_{\text{recent}}$ ) =  $G$  then
20:     $\hat{V}_{\text{new}} \leftarrow \text{Quantize}(V_{\text{recent}}[:, G])$ 
21:     $V_{\text{recent}} \leftarrow V_{\text{recent}}[G : ]$ 
22:     $\hat{V}_{\text{cache}} \leftarrow \text{concat}(\hat{V}_{\text{cache}}, \hat{V}_{\text{new}})$ 
23:
24:  end if
25:  return  $O$ 
26: end procedure
```

▷ **Prepare Inputs**  
▷  $Q \in \mathbb{R}^{1, d}$   
▷  $V \in \mathbb{R}^{1, d}$   
▷  $V \in \mathbb{R}^{1, d}$

▷ **Compute Output**

▷ **Quantize New Tokens**

---

## A Attention Computation using InnerQ

Algorithms 1 and 2 describe the process of computing the attention using InnerQ in the prefill and decode phases. We use a notation similar to PyTorch for indexing matrices in these algorithms.

## B Full Latency Results

We report the measured latencies corresponding to the speedups in Figures 3a and 3b in Tables 3 and 4, respectively.

---

**Algorithm 2** Multi-head attention with quantized cache in the prefill phase

---

**Require:** Input sequence  $X \in \mathbb{R}^{N \times d}$ **Require:** Trainable weights  $W_Q, W_O, W_K, W_V \in \mathbb{R}^{d \times d}$ **Require:** Number of heads  $n_h$  and head dimension  $d_h = d/n_h$ **Require:** Quantization Group Size  $G$ 

```
1: procedure LLAMA3ATTENTION( $X$ )
2:
3:    $Q \leftarrow XW_Q$ 
4:    $K \leftarrow XW_K$ 
5:    $V \leftarrow XW_V$ 
6:    $Q, K \leftarrow \text{ApplyRoPE}(Q, K)$ 
7:
8:    $S \leftarrow QK^\top$ 
9:    $P \leftarrow \text{Softmax}((S/d_h) + \text{Mask})$ 
10:   $O \leftarrow PVW_O$ 
11:
12:   $K_{\text{sink}} \leftarrow K[:w_{\text{sink}}]$ 
13:   $K_{\text{recent}} \leftarrow K[-w_{\text{recent}}:]$ 
14:   $\hat{K}_{\text{cache}} \leftarrow K[w_{\text{sink}}:-w_{\text{recent}}]$ 
15:   $V_{\text{sink}} \leftarrow V[:w_{\text{sink}}]$ 
16:   $V_{\text{recent}} \leftarrow V[-w_{\text{recent}}:]$ 
17:   $\hat{V}_{\text{cache}} \leftarrow V[w_{\text{sink}}:-w_{\text{recent}}]$ 
18:   $\text{norm}^K \leftarrow \sqrt{\max(|K|, \text{dim} = 0)}$ 
19:   $W_K \leftarrow W_K/\text{norm}^K$ 
20:   $W_Q \leftarrow W_Q \times \text{norm}^K$ 
21:  return  $O$ 
22: end procedure
```

▷ **Prepare inputs**  
▷  $Q \in \mathbb{R}^{N,d}$   
▷  $K \in \mathbb{R}^{N,d}$   
▷  $V \in \mathbb{R}^{N,d}$

▷ **Compute output**

▷ **Initialize the quantized KV cache**

▷  $\text{norm}^K \in \mathbb{R}^d$   
▷ Future tokens are automatically normalized

---

Model	Method	512	1024	2048	4096	8192	16384	32768	65536	131072
Llama 3.2-1B	torch.matmul	0.024	0.036	0.059	0.106	0.268	0.608	1.226	2.392	4.671
	Inner Dim. Quantization	0.008	0.009	0.014	0.023	0.040	0.074	0.141	0.274	0.541
	Speedup	67.86%	75.46%	76.00%	78.67%	85.10%	87.87%	88.51%	88.53%	88.41%
Llama 3.1-8B	torch.matmul	0.036	0.058	0.106	0.268	0.606	1.226	2.391	4.669	9.390
	Inner Dim. Quantization	0.009	0.014	0.023	0.040	0.074	0.141	0.274	0.541	1.077
	Speedup	74.23%	76.65%	78.50%	84.92%	87.85%	88.50%	88.53%	88.41%	88.53%
Llama 2-13B	torch.matmul	0.043	0.070	0.145	0.340	0.737	1.517	2.920	5.838	11.725
	Inner Dim. Quantization	0.012	0.017	0.027	0.048	0.090	0.175	0.341	0.677	1.343
	Speedup	72.00%	75.64%	81.07%	85.77%	87.73%	88.48%	88.32%	88.41%	88.54%

Table 3: Latency of the vector-matrix multiplication using 2-bit quantization when grouped over the inner dimension and torch.matmul on half-precision data. The latencies are reported in milliseconds.

Model	Method	512	1024	2048	4096	8192	16384	32768	65536	131072
Llama 3.2-1B	Outer Dim. Quantization	0.009	0.010	0.016	0.028	0.051	0.095	0.181	0.354	0.703
	Inner Dim. Quantization	0.008	0.009	0.014	0.023	0.040	0.074	0.141	0.275	0.542
	Speedup	15.91%	15.10%	14.21%	19.02%	21.15%	22.16%	22.14%	22.16%	22.87%
Llama 3.1-8B	Outer Dim. Quantization	0.010	0.016	0.027	0.050	0.095	0.182	0.354	0.703	1.388
	Inner Dim. Quantization	0.009	0.014	0.023	0.040	0.074	0.142	0.275	0.542	1.075
	Speedup	11.37%	14.58%	15.23%	19.50%	21.74%	22.04%	22.41%	22.86%	22.54%
Llama 2-13B	Outer Dim. Quantization	0.014	0.020	0.033	0.062	0.116	0.225	0.441	0.875	1.730
	Inner Dim. Quantization	0.012	0.017	0.027	0.049	0.090	0.175	0.342	0.675	1.344
	Speedup	15.51%	16.07%	18.35%	21.13%	22.41%	22.15%	22.47%	22.79%	22.32%

Table 4: Latency of the vector-matrix multiplication using 2-bit quantization when grouped over the inner or the outer dimension. The latencies are reported in milliseconds.